Supporting Information

Fluorine-free Polysiloxane-based Single-Ion Conducting Polymer Electrolyte for Lithium-Metal Batteries

Leo Gräber[†,‡], Vittorio Marangon[†,‡,*] Manish Kumar[†,‡] , Marcel Weil[†,‡], and Dominic Bresser[†,‡,§,*]

[†]*Helmholtz Institute Ulm (HIU), Helmholtzstrasse 11, 89081 Ulm, Germany*

[‡]*Karlsruhe Institute of Technology (KIT), P.O. Box 3640, 76021 Karlsruhe, Germany*

[§] *Ulm University (UUlm), 89069 Ulm, Germany*

***Corresponding authors:** vittorio.marangon@kit.edu ; dominic.bresser@kit.edu

Experimental

1. Materials

Azobisisobutyronitrile (AiBN), malononitrile, polyacrylonitrile (PAN, M_W = 150 kg mol^{-1}), propylene carbonate (PC, > 99%, H_2O < 10 ppm) and sodium *p*-styrenesulfonate salt were purchased from Sigma-Aldrich. Acetonitrile (MeCN), lithium hydroxide monohydrate (LiOH), *N,N*-dimethylformamide (DMF), tetrahydrofurane (THF), thionylchloride and triethylamine (TEA) were purchased from Thermo Fisher, acetone and dichloromethane (DCM) from VWR chemicals, *tert*-butylcatechol from Acros Organics, poly[(mercaptopropyl)methylsiloxane] (PMMS, M_W = 4000-7000 g mol^{-1}, 75-150 cSt) from Gelest, $LiFePO_4$ (LFP, carbon-content 2-3 %) from Süd-Chemie, carbon black C45 from Imerys and sodium carboxymethyl cellulose (CMC) from Dow Chemical Company. All materials were used as received, except for AiBN, which was recrystallized twice before use.

2. Synthesis of LiSDM

Lithium (4-styrenesulfonyl)(dicyano)methide (LiSDM) was synthesized via a modified procedure reported by Martinez-Ibanez et al.[1] An oven-dried 100 mL Schlenk-flask equipped with a magnetic stirrer and a reflux condenser was filled with 14 mL of DMF under argon atmosphere and cooled down to 0 °C. Subsequently, 10.3 mL (142 mmol, 5.7 eq.) of thionylchloride was added using a syringe, followed by 80 mg (0.5 mmol, 0.02 eq.) of tert-butylcatechol. After stirring for 10 min, 6.67 g (32.3 mmol, 1.3 eq.) of sodium p-styrenesulfonate salt was added over a time interval of 15 min and the solution was stirred overnight. The mixture was then poured slowly in 40 mL of ice-cooled water to quench the remaining thionylchloride, followed by extraction with 3×20 mL of DCM. The collected organic phases were washed with 10 mL of deionized water and a saturated aqueous sodium chloride solution. The solvent was removed under vacuum after drying over $MgSO_4$ crystals. The final product appeared as a yellow-colored oil (4.91 g, 1.0 eq., yield: 75%) that was used without further purification by dissolving it in 40 mL of anhydrous MeCN in a 250 mL two-neck Schlenk-

flask equipped with a magnetic stirrer, a reflux condenser and a rubber septum under argon atmosphere. Afterwards, 1.76 g (26.6 mmol, 1.1 eq.) of Malononitrile was added using a syringe prior to be cooled to 0 °C. Under stirring, 16.9 ml of TEA (121.1 mmol, 5 eq.) was added and the mixture was stirred overnight. The solvent was removed under vacuum and the resulting product was dissolved in 250 mL of 1M LiOH (4 eq.) solution under stirring for 1 h. The solution was acidified by dropwise adding H_2SO_4, and extracted with 3×100 ml DCM. The solvent was once more removed under vacuum to dissolve the product in 100 ml of a 4M LiOH solution, which was then stirred overnight. Excess water was removed via vacuum. The product was dissolved in MeCN and separated from residual LiOH by filtration. After the complete removal of the solvent by vacuum, 4.67 g of the final product were obtained as a slightly yellow solid with an 81% yield. The composition of the obtained LiSDM was verified by ^{13}C NMR spectroscopy performed in deuterium oxide at 300 MHz.

3. Synthesis of the SIPE

The SIPE was synthesized via a thiol-ene click reaction as previously reported for similar substrates.[2] Accordingly, 2.38 g (10.0 mmol) of LiSDM was dissolved in 20 mL of anhydrous THF alongside with 1.34 g of PMMS and 68 mg (0.4 mmol) of AiBN in a 100 mL Schlenk flask equipped with a magnetic stirrer and a reflux condenser under argon atmosphere. The mixture was stirred for 12 h at 65 °C. Afterwards, the solvent was removed by applying a vacuum and the product was dissolved in a minimum amount of acetone. 2.78 g SIPE was obtained as a pale-yellow powder with a 75% yield by precipitation in DCM, separation via centrifugation and final drying in vacuum. The molecular weight of the final SIPE was determined by gel permeation chromatography (GPC, Omnisec Reveal, Malvern Panalytical) and the results are reported in **Table S1**.

Table S1. Molecular weight values measured for the SIPE by GPC.

M_n [g mol^{-1}]	M_w [g mol^{-1}]	M_z [g mol^{-1}]	M_w / M_n
10,300 ± 500	13,700 ± 600	19,900 ± 900	1.33 ± 0.01

4. Membrane Preparation and Characterization

Polymer blends including different PAN contents were prepared by solvent casting. 400 mg of the polymer mixture (SIPE+PAN, see also **Table S2**) were dissolved in 8 mL of DMF in a screw-cap vial and stirred for about 24 – 48 h, before carefully decanting in a Petri dish with a diameter of 4.5 cm. The solvent was slowly evaporated at 50 °C in a vacuum-oven. The resulting films were punched into membranes with a diameter of 14 mm, which were dried at 80 °C in high vacuum (< 10^{-2} mbar) for 24 h. The final thickness of the membranes ranged between 100 and 150 µm. A second batch with a thickness ranging between 180 and 200 µm was produced for comparison. X-ray diffraction (XRD) patterns for bare PAN, the SIPE powder, and the dry B35 membrane were collected in the 10 – 90° 2θ range, applying a step size of 0.03° and a rate of 0.65 s per step, using a Bruker D8 Advance. Scanning electron microscopy (SEM) and energy dispersive X-ray spectroscopy (EDX) were performed on the dry B35 membrane using a ZEISS Crossbeam XB340 microscope coupled with an Ultim Extreme™ (Oxford instruments) EDX spectrometer operating at 5 kV. The dry membranes were soaked with PC (50 wt.% with respect to membrane weight) in a dry room (dew point: ca. -80 °C) and subsequently sandwiched between two Mylar foils and sealed in a pouch bag for 48 h. The PC solvent content of 50 wt.% in the final polymer electrolyte membranes was confirmed by the weight ratio of the dry membranes and the soaked ones (Equation S1). Thermogravimetric analysis (TGA) was performed under a N_2 flow of 20 mL min^{-1} between 40 and 500 °C at a heating rate of 5 K min^{-1} using a Discovery TGA 1 from TA instruments to assess the actual SIPE:PAN ratio, the decomposition temperature of the membranes, and the PC solvent content. To determine the PC content, the sample was kept at a relevant N_2 flow of 50 mL min^{-1} at 100 °C for 6 h to allow for the complete evaporation of the solvent.

Table S2. Acronyms and corresponding compositions of the obtained SIPE:PAN membranes.

Acronym	SIPE:PAN ratio (wt.%)
B15	85:15
B25	75:25
B35	65:35
B45	55:45
B55	45:55

$$solvent\ content = 100\% \cdot \frac{m_{dry}}{m_{soaked}} \quad \text{(S1)}$$

5. Fabrication of LFP-based Electrodes

LFP-based electrodes were prepared via doctor blade casting of the electrode slurry onto a battery-grade carbon-coated aluminum foil (Wellcos Corporation). The first batch of electrodes was prepared using an aqueous slurry composed of 82 wt.% LFP, 10 wt.% carbon black C45 and 8 wt.% CMC as polymeric binder. The CMC was used in a deionized water solution at 40 wt.% which served in addition as dispersing solvent. The electrode tapes were dried in oven at 80 °C upon casting, punched into discs with a diameter of 12 mm (area: 1.13 cm^2) and dried at 80 °C under high vacuum (< 10^{-2} bar) in a Büchi oven for 24 h before transferring in an Ar-filled glovebox (MBraun, H_2O and O_2 content below 1 ppm). The final LFP areal loading of the first batch of electrodes was (2.8 ± 0.2) mg cm^{-2}. A second batch of electrodes was prepared with a final LFP areal loading of either 8.2 or 9.2 mg cm^{-2} following the same pathway, while using a slurry composed of 82 wt.% LFP, 6 wt.% carbon black C45, 5 wt.% CMC and 7 wt.% of dry SIPE. The high loading electrodes of the second batch were in addition pressed at 4300 bar for 10 s through a hydraulic press prior to the final drying step in Büchi oven.

6. Electrochemical Tests

All the electrochemical tests were performed using CR2032 coin-type cells (Hohsen) assembled in an Ar-filled glovebox (MBraun, H_2O and O_2 content below 1 ppm). All isothermal electrochemical tests were performed in climatic chambers at 40 °C. Lithium metal discs with a diameter of 12 mm and a thickness of 500 μm were used. The ionic conductivity (σ) of the polymer electrolyte membranes was determined by electrochemical impedance spectroscopy (EIS) performed on symmetric stainless-steel‖stainless-steel cells in the 1.0 MHz – 1 Hz frequency range (voltage amplitude: 10 mV) between 90 and 10 °C (cooling trend). The cells were allowed to rest for 3 h at every selected temperature prior to the EIS measurement. The temperature was controlled via a climatic chamber. The resulting Nyquist plots were fitted using the non-linear least squares (NLLS) method via the RelaxIS 3 software to determine the electrolyte resistance (R_e). Possible middle-frequency semicircles due to grain boundary or heterogeneity contributions in the polymer membranes at low temperatures were not considered for the fitting. The anodic stability of the membranes was evaluated by linear sweep voltammetry (LSV) carried out using Li‖stainless-steel cells between the open circuit voltage (OCV) and 6.0 V vs. Li^+/Li at a sweep rate of 0.1 mV s^{-1}. The value of the anodic potential limit was determined in correspondence to the development of a current of 2.5 μA cm^{-2}. Lithium stripping/plating tests were performed using symmetric Li‖Li cells via galvanostatic cycling at increasing current densities of 2.5, 5.0, 10, 20, 50 and 100 μA cm^{-2}, incremented every 10 cycles and setting a step time between charge and discharge of 30 min. The following electrochemical measurements were performed exclusively with the B35 polymer electrolyte membranes. The stability of B35 upon aging in symmetric Li‖Li cells was evaluated by carrying out EIS between 200 kHz and 50 mHz (voltage amplitude: 10 mV) every 2 h after cell assembly for 12 h and subsequently every day for 7 days. The resulting Nyquist plots were analyzed via the NLLS fitting method using the Boukamp software and exclusively accepting fits with a χ^2 value of the order of 10^{-4} or lower.[3,4] The fitting was performed using a $R_e(R_iQ_i)(R_wQ_w)$ equivalent circuit, where R and Q represent resistive and constant phase elements, respectively. In particular, R_e

indicates the electrolyte bulk resistance, (R_iQ_i) identifies the high-middle frequency semicircle in the Nyquist plots of which the width measures the electrode/electrolyte interphase resistance (R_i), and (R_wQ_w) defines the low frequency semicircle associated with the Li^+ ions finite-length Warburg-type diffusion. After aging, the same Li‖Li cells were subjected to a Li stripping/plating test, setting a step time of 30 min between charge and discharge and increasing the current density from 10 to 50 μA cm^{-2}, while EIS tests were performed between 200 kHz and 50 mHz (voltage amplitude: 10 mV) after 5, 10, and 55 cycles. The resulting Nyquist plots were analyzed via the NLLS fitting method using a $R_e(R_iQ_i)(R_wQ_w)$ equivalent circuit. A long-term Li stripping/plating test was performed on symmetric Li │ B35 │ Li cells at 50 μA cm^{-2} by setting a step time between charge and discharge of 30 min. The Li^+ transference number (t^+) of B35 was evaluated using the Bruce-Vincent-Evans method.[5] Accordingly, a chronoamperometric test was carried out by applying a voltage amplitude (ΔV) of 10 mV for 180 min on Li │ B35 │ Li cells using a B35 membrane with a thickness of either 120-130 μm or 180- 200 μm, and EIS tests were performed between 200 kHz and 50 mHz (voltage amplitude: 10 mV) before and after polarization. The resulting Nyquist plots were fitted via the NLLS method with a $R_e(R_iQ_i)(R_wQ_w)$ equivalent circuit model to measure the electrode │electrolyte interphase resistance using the Boukamp software. The value of t^+ was calculated using equation S2:[5]

$$t^+ = \frac{i_{ss}}{i_0} \times \frac{(\Delta V - R_0 i_0)}{(\Delta V - R_{ss} i_{ss})} \qquad \text{(S2)}$$

where i_0 and i_{ss} are the current values at the initial and final stage (steady state) of the chronoamperometric test, while R_0 and R_{ss} are the electrode │electrolyte resistance values before and after polarization. Rate capability tests were performed by galvanostatic cycling measurements on Li │ B35 │ LFP cells by increasing the C rate (1C = 170 mA g^{-1}) from 0.05C to 0.1C, 0.2C, 0.5C, 1C, and 2C every 5 cycles and decreasing the current back to 0.2C after 30 cycles within the 2.5 – 4.0 V voltage range. The same voltage range was employed for long-term galvanostatic cycling

measurements, which were ran at a constant C rate of either 0.2C or 0.5C. Prior to the long-term cycling, the cells were subjected to either 1 or 3 activation cycles at 0.05C between 2.5 and 4.0 V. Additional cycling of Li │B35│LFP was performed at 20 °C at 0.5C between 2.5 and 4.0 V. EIS spectra were recorded before cycling after 12 h of rest between 200 kHz and 50 mHz using a voltage signal amplitude of 10 mV. The Nyquist plot was analyzed via the NLLS fitting method, using the $R_e(R_iQ_i)Q_g$ equivalent circuit and the Boukamp software, where Q_g is the geometric capacitance of the cell represented by the vertical low-frequency line. EIS was also carried out at OCV and upon cycling for Li │B35│LFP cells (at 0.5C with 3 activation cycles at 0.05C, 2.8 mg cm^{-2}) in the 200 kHz – 50 mHz frequency range with a voltage amplitude of 10 mV. The resulting Nyquist plots were analyzed via NLLS fitting using the $R_e(R_iQ_i)Q_w$ equivalent circuit and the Boukamp software.

EIS data for the determination of the ionic conductivity were recorded with a Solartron Impedance Analyzer (ModuLab XM MTS, Ametek Scientific Instruments), while EIS for the lithium cells, potentiostatic measurements and Li stripping/plating galvanostatic tests were performed using a BioLogic VMP 3e. A Maccor series 4000 battery test instrument was used for the Li stripping/plating, rate capability tests, and long-term galvanostatic cycling.

7. Hazard and Toxicity Screening

To assess the toxicity of the SIPE membrane and of a F-containing analogous studied previously, i.e., PSiOM,[2] a hazard and toxicity screening approach was adopted, which addresses the EU "safe and sustainable by design" (SSbD) concept and the general approach to include such aspects already at early stages of the technology design phase.[6,7] These assessments include qualitative hazard traffic lights (HTL) and quantitative total hazard points (THP) methodologies. HTL uses colour codes to represent hazards statements associated with materials and chemicals such as red for warning and yellow for danger. Colour codes associated with each H-code can be sourced from an earlier study.[8] The hazard statements include three hazard classes (physical, health, and environmental) and 28 sub-classes (e.g., explosives, flammable liquids, eye damage, carcinogenicity, hazardous to aquatic

environment, etc.). Each hazard statement is associated with an H-code (represented as H*xxx*, i.e., H followed by 3 numbers). A limited HP methodology was initially developed by the German Environmental Agency (UBA). Hazard points are calculated from the quantity thresholds, i.e., the lower tier (LT) value (in tons) associated with each H-code, which if exceeded, requires special safety conditions as per the major accident prevention policy (MAPP). THP are calculated as the sum of all HP, i.e., the mass share of all precursors respective to the LT values for an overall comparative hazard and toxicity performance of alternatives. The detailed methodology and the mathematical calculations can be found in earlier published studies.[6,8] Both HTL and THP approaches are in line with the SSbD concept to minimize the use of hazardous chemicals and materials.[9,10] HTL are identified by extracting H-codes for the CAS numbers from the European Chemicals Agency (ECHA) chemicals database.[11] HTL includes all classified H-codes as well as the harmonized ones based on the classification and labelling (C&L) notifications submitted to ECHA. The information contained in the C&L inventory is provided by companies in the respective classification notifications or registration dossiers. An HTL assessment was conducted for SIPE and PSiOM electrolytes with the consideration of all precursors involved in the synthesis, i.e., for SIPE the *(i)* synthesis of the (4-styrene)sulfonylchloride, *(ii)* synthesis of the LiSDM ionic side-chain, *(iii)* synthesis of the SIPE powder, and (*iv)* membrane preparation, while for PSiOM the *(i)* sulfochlorination of the starting material, *(ii)* synthesis of lithium 1-[3-(methacryloyloxy)-propylsulfonyl]-1-(trifluoromethylsulfonyl)imide, *(iii)* synthesis of the PSiOM single-ion conducting polymer, and *(iv)* membrane fabrication. In the case of missing classified notifications for some chemicals (e.g., lithiumhydroxide monohydrate in 'synthesis of the LiSDM ionic side-chain' and dimethylsulfoxide in 'PSiOM membrane fabrication'), the submitted C&L information with a minimum of 100 notifiers was considered, following the assumptions made in an earlier study.[6] Furthermore, THP were also calculated for each input chemical as well as the mixtures in the sub-processes to perform a comparison of SIPE with the PSiOM ionomer. However, due to the incomplete classification of

chemicals involved in both cases, resulting in higher uncertainty, a comparative THP evaluation of two electrolytes was not feasible.

Figure S1 shows the ^{13}C NMR spectrum of the LiSDM ionic side-chain. The successful lithiation of the (4-styrene)sulfonylchloride (see schematic representation of synthesis pathway in **Figure 1**) is indicated by the signal at 42.17 ppm, i.e., C_8, which identifies the negatively charged methide carbon.[1]

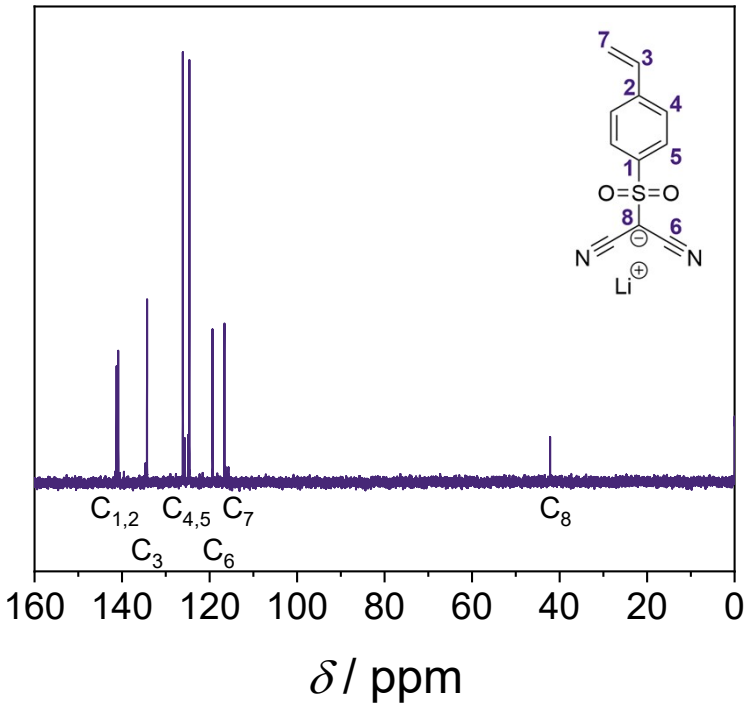

Figure S1. ^{13}C NMR spectrum of LiSDM recorded in deuterium oxide at 300 MHz.

Figure S2 shows a photograph of one of the final polymer electrolyte membranes obtained by mixing SIPE membranes with various amounts of PAN. The membranes were indicated in the text as B15, B25, B35, B45 and B55 (see the corresponding composition in **Table S2**). The final thickness ranged between 100 and 150 μm. The use of PAN was fundamental to achieve self-standing membranes.

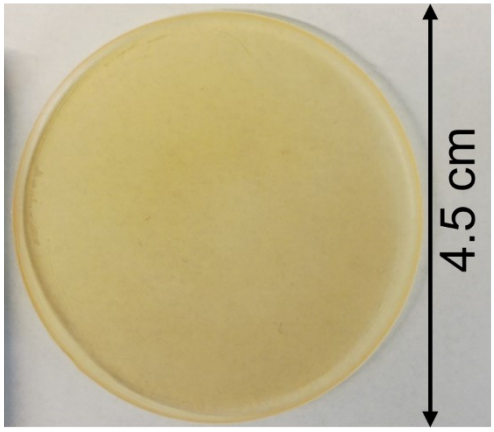

Figure S2. Photograph of a B35 membrane captured after casting.

Figure S3a displays the TGA data obtained for the dry B15-B55 membranes, the neat SIPE and bare PAN to evaluate the decomposition temperatures. The trend reported in **Figure 2**a reveals the gradual increase of the decomposition temperature concomitant with the increase of the PAN content. **Figure S3**b reports an example of a TGA measurement performed on B35 to assess the residual PC content, which is determined to be of 50 wt.% with respect to each membrane (a further confirmation of this value is obtained through Equation S1).

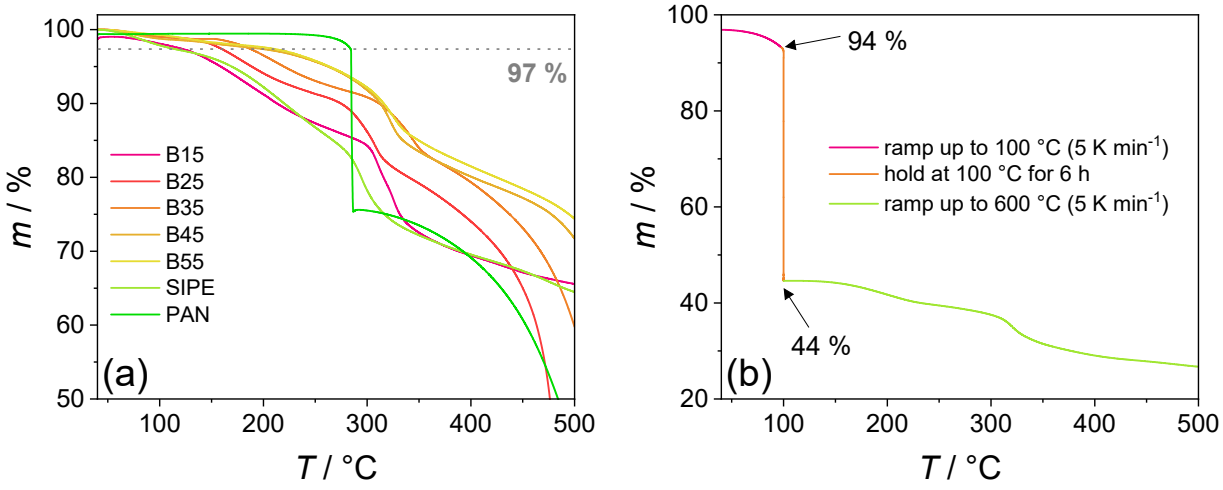

Figure S3. TGA data of **(a)** dry B15-55 membranes, the neat SIPE, and PAN to determine the decomposition temperatures (see corresponding plot in **Figure 2a**) and of **(b)** a B35 membrane previously soaked with PC to confirm the solvent content of 50 wt.% with respect to the membrane. The measurements were carried out using a heating rate of 5 K min^{-1} between 40 and 500 °C.

Figure S4 shows the Nyquist plots obtained by EIS performed on symmetric stainless-steel ‖ stainless-steel cells at various temperatures to determine the ionic conductivity of the B15-B55 polymer electrolyte membranes. The corresponding Arrhenius plots are presented in **Figure 2**c.

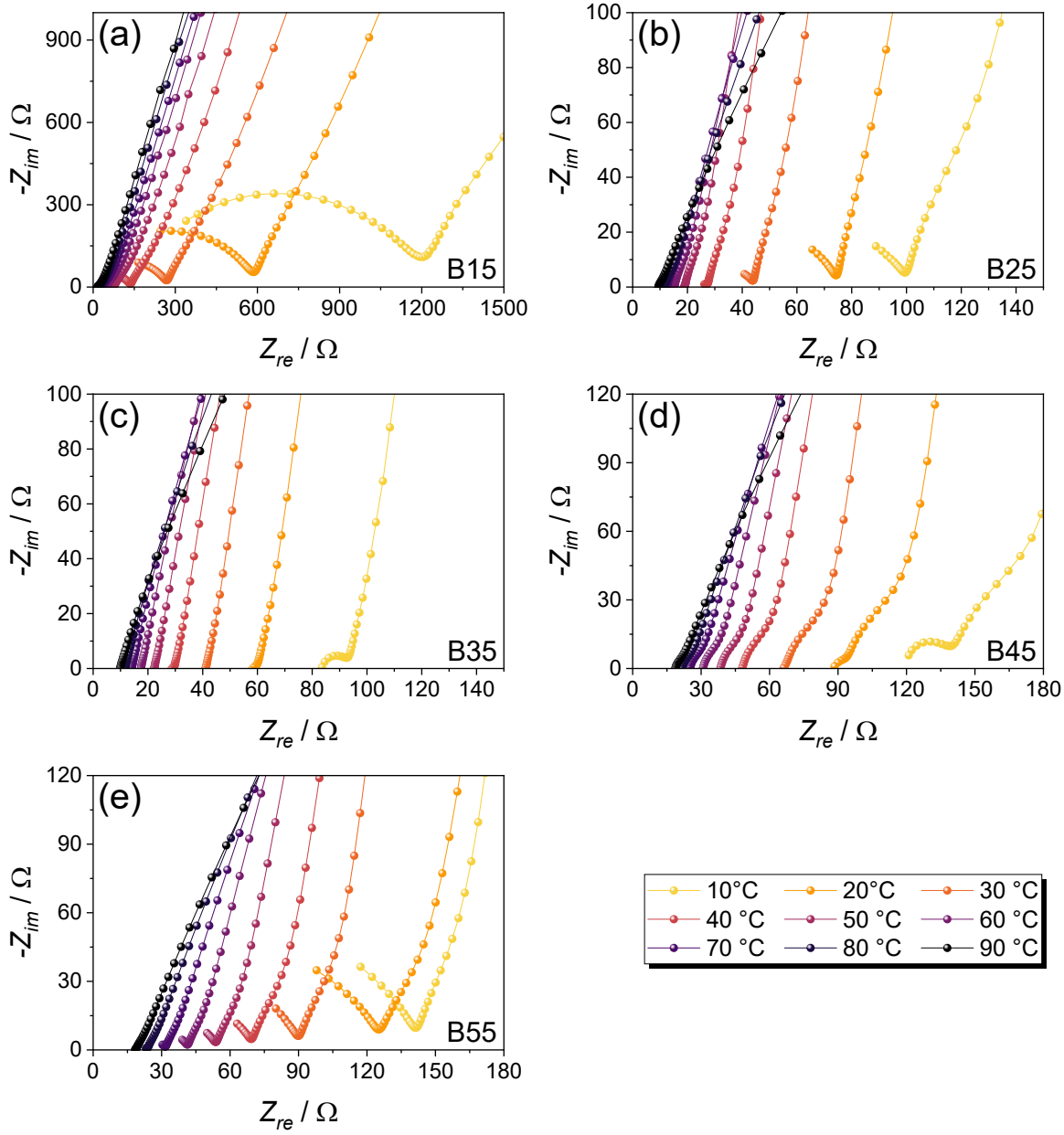

Figure S4. Nyquist plots recorded via EIS on blocking-electrode stainless-steel ‖ stainless-steel cells to determine the ionic conductivity of the **(a)** B15, **(b)** B25, **(c)** B35, **(d)** B45, and **(e)** B55 membranes between 10 and 90 °C in the 1.0 MHz – 1 Hz frequency range with a voltage amplitude of 10 mV (see the corresponding Arrhenius plot in **Figure 2**c).

Figure S5 reports the voltage profiles of the galvanostatic Li stripping/plating tests performed on symmetric Li‖Li cells containing the B15-B55 membranes at 40 °C at increasing current densities from 2.5 to 100 μA cm^{-2}. B35 shows the lowest overpotential. A comparison of the overpotential vs. the current density is presented in **Figure 2d**.

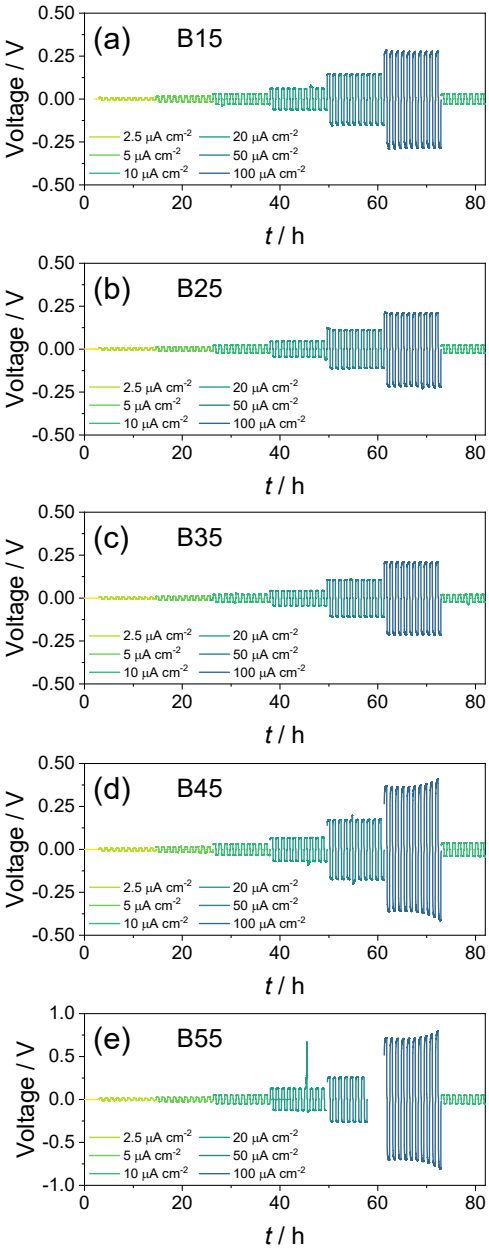

Figure S5. Voltage profiles of the lithium stripping/plating tests performed at increasing current densities on symmetric Li‖Li cells containing **(a)** B15, **(b)** B25, **(c)** B35, **(d)** B45, or **(e)** B55 at 40 °C. The step time between charge and discharge was 30 min.

Figure S6 shows the XRD patterns collected for bare PAN, the SIPE powder, and the dry B35 membrane. The measurements reveal the suitable blending of the two polymers in B35, as indicated by the coexistence of the amorphous structure of the SIPE and the crystalline features of PAN.

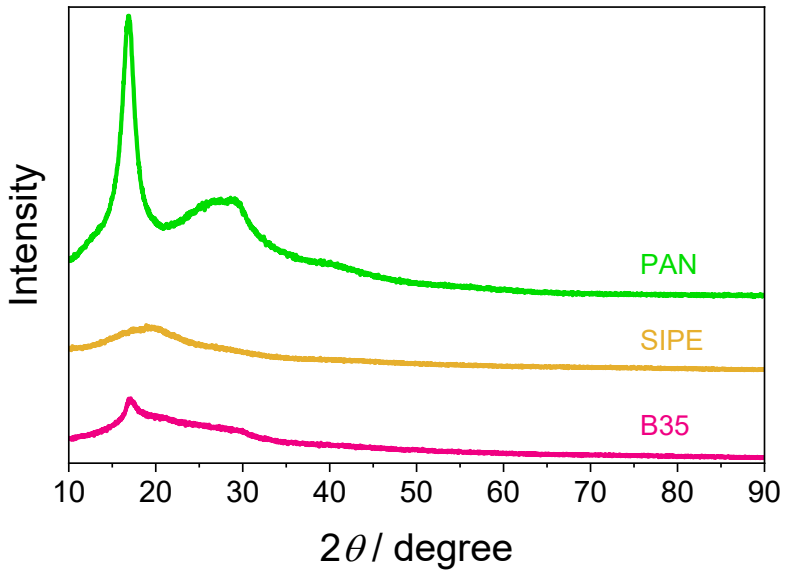

Figure S6. XRD patterns of bare PAN, the SIPE powder, and a dry B35 membrane, measured in the 10 – 90° 2θ range.

The t^+ of the B35 membrane is determined in **Figure S7** via the Bruce-Vincent-Evans method applied on two different symmetric Li‖Li cells (panels a and b) using different thicknesses of the electrolyte membrane, i.e., either 120-130 µm or 180-200 µm, to corroborate the suitability of the calculation.[5] The figure shows the chronoamperometric curve obtained upon polarization of the cells and the Nyquist plots recorded by EIS before and after chronoamperometry (inset). The obtained data are displayed in **Table S3** and used in Equation S2 to calculate t^+ which presents in both cases a value of around 1, as expected by the single-ion conducting nature of the membrane even by increasing the B35 thickness by 50%, although a slight overestimation deriving from the method applied acnnot be excluded.

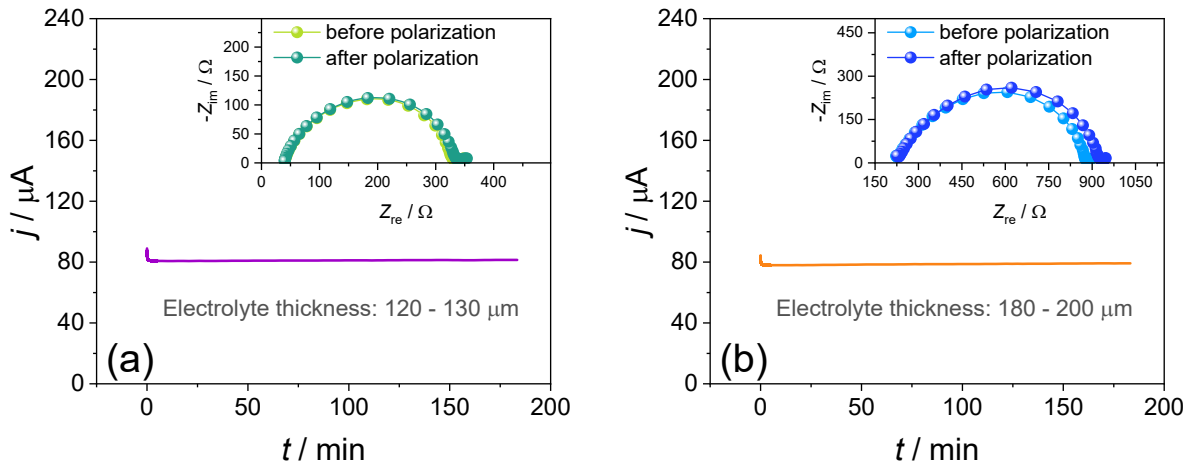

Figure S7. Chronoamperometric curves recorded for two symmetric Li‖Li cells using B35 with different thicknesses (panels a and b) and Nyquist plots recorded by EIS before and after polarization (insets) to determine t^+ at 40 °C using the Bruce-Vincent-Evans method (see Experimental section for details and **Table S3** for the employed parameters). Polarization voltage: 10 mV. EIS frequency range: 200 kHz – 100 mHz. Voltage amplitude: 10 mV.

Table S3. Parameters used to calculate t^+ from the data presented in **Figure S7** using the Bruce-Vincent-Evans method (see Equation S2) for two different symmetric Li‖Li cells using B35 (entries a and b). The fitting of the Nyquist plots was carried out using the $R_e(R_iQ_i)(R_wQ_w)$ equivalent circuit to evaluate the interphase resistance (R_i).

Entry	ΔV [V]	i_0 [A]	i_{ss} [A]	R_0 [Ω]	R_{ss} [Ω]	t^+
(a)	0.01	8.9×10^{-5}	8.1×10^{-5}	295	301	1.0
(b)	0.01	8.4×10^{-5}	7.9×10^{-5}	668	714	0.93

The NLLS analyses performed on the Nyquist plots displayed in **Figure 3**g are reported in **Table S4**. The electrode│electrolyte interphase resistance (R_i) evolution shows the development and consolidation of a low resistive SEI for the Li │B35 │Li cells upon calendar aging at 40 °C. The R_i vs. time trend is depicted in **Figure 3**i.

Table S4. NLLS fitting outcomes of the Nyquist plots reported in **Figure 3**a recorded upon calendar aging of symmetric Li │B35 │Li cells at 40 °C.

Aging time	**Circuit**	R_i **[Ω]**	χ^2
2 h	$R_e(R_iQ_i)(R_wQ_w)$	211 ± 1	1×10^{-4}
4 h	$R_e(R_iQ_i)(R_wQ_w)$	213 ± 1	9×10^{-5}
6 h	$R_e(R_iQ_i)(R_wQ_w)$	216 ± 1	9×10^{-5}
8 h	$R_e(R_iQ_i)(R_wQ_w)$	219 ± 1	8×10^{-5}
10 h	$R_e(R_iQ_i)(R_wQ_w)$	222 ± 1	9×10^{-5}
12 h	$R_e(R_iQ_i)(R_wQ_w)$	225 ± 1	9×10^{-5}
1 day	$R_e(R_iQ_i)(R_wQ_w)$	237 ± 1	1×10^{-4}
2 days	$R_e(R_iQ_i)(R_wQ_w)$	254 ± 1	1×10^{-4}
3 days	$R_e(R_iQ_i)(R_wQ_w)$	265 ± 1	1×10^{-4}
4 days	$R_e(R_iQ_i)(R_wQ_w)$	275 ± 1	1×10^{-4}
5 days	$R_e(R_iQ_i)(R_wQ_w)$	284 ± 1	1×10^{-4}
6 days	$R_e(R_iQ_i)(R_wQ_w)$	291 ± 1	1×10^{-4}
7 days	$R_e(R_iQ_i)(R_wQ_w)$	298 ± 1	1×10^{-4}

Table S5. NLLS analyses of the Nyquist plots displayed in Figure S7 acquired at 40 °C by EIS upon Li stripping/plating test performed on a symmetric Li │ B35 │ Li cell after aging (see **Figure 3**).

Cell condition	**Circuit**	R_i **[Ω]**	χ^2
After 5 cycles at 10 μA cm^{-2}	$R_e(R_iQ_i)(R_wQ_w)$	304 ± 1	1×10^{-4}
After 5 cycles at 50 μA cm^{-2}	$R_e(R_iQ_i)(R_wQ_w)$	306 ± 1	1×10^{-4}
After 50 cycles at 50 μA cm^{-2}	$R_e(R_iQ_i)(R_wQ_w)$	308 ± 1	1×10^{-4}

After aging at 40 °C (see **Figure 3**g, h), the symmetric Li │B35 │Li cell was subjected to galvanostatic Li stripping/plating tests at increasing current density and EIS tests, as reported in **Figure S8**. Despite the cycling (**Figure S8**a, b) the Nyquist plots recorded by EIS suggest remarkable stability of the electrode/electrolyte interphase resistance (**Figure S8**c), as confirmed by the corresponding NLLS analyses in **Table S5** which show barely increasing values of about 300 Ω.

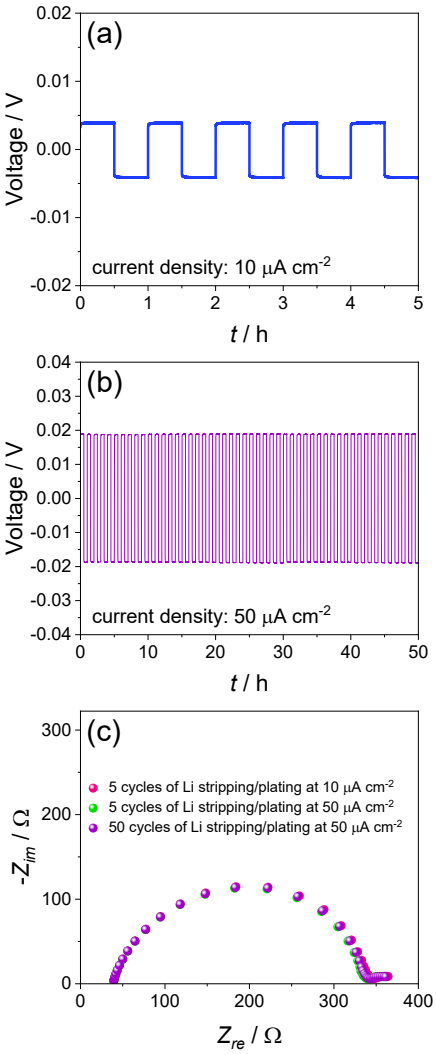

Figure S8. (a, b) Voltage profiles recorded via galvanostatic Li stripping/plating performed at **(a)** 10 μA cm^{-2} and **(b)** 50 μA cm^{-2} at 40 °C in symmetrical Li │B35 │Li cells after aging (see **Figure 3**g,h), and **(c)** Nyquist plots obtained through EIS upon cycling (see **Table S5** for NLLS analyses). Step time between charge and discharge: 30 min. EIS frequency range: 200 kHz – 50 mHz. Voltage amplitude: 10 mV.

The single-ion conducting character of the B35 membrane is further evidenced by **Figure S9**, which reports the magnification of the voltage profiles related to the Li stripping/plating test displayed in **Figure 3**i. The profiles show the expected squared shape of the stripping/plating plateaus, where the slight slope observed is attributed to the Li^+ transport across the SEI layer, which slows down the Li^+ migration.

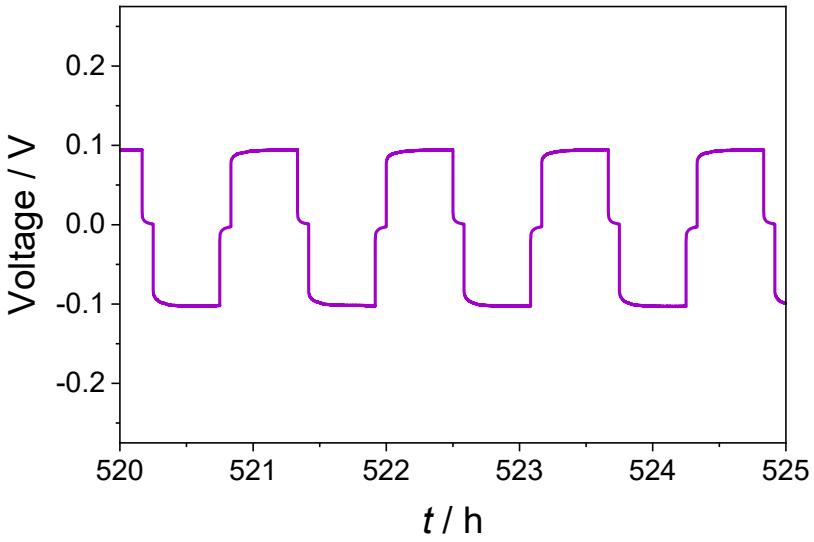

Figure S9. Magnification of the voltage profiles related to the long-term Li stripping/plating experiment depicted in **Figure 3**i.

Table 6 shows the NLLS analyses of the Nyquist plots reported in **Figure 5**g, which were recorded on Li │ B35 │ LFP cells upon cycling. The R_i values display an initial consolidation of the passivation layers during the activation cycles, a subsequent dissolution with concomitant resistance drop, and a constant increase until the end of the test, which is attributed to the continuous growth of the resistive passivation layers at the electrode surfaces. The R_i trend as function of cycle number is depicted in **Figure 5**h.

Table S6. NLLS analyses of the Nyquist plots recorded on Li|B35|LFP cells, cycled at 0.5C with 3 activation cycles at 0.05C (T = 40 °C). The corresponding Nyquist plots are reported in **Figure 5**g, and the corresponding trend of R_i in **Figure 5**h.

Condition	**Circuit**	R_i **[Ω]**	χ^2
OCV	$R_e(R_iQ_i)Q_w$	317 ± 2	3×10^{-5}
After 3 cycles	$R_e(R_iQ_i)Q_w$	327 ± 5	2×10^{-4}
After 5 cycles	$R_e(R_iQ_i)Q_w$	257 ± 3	7×10^{-5}
After 25 cycles	$R_e(R_iQ_i)Q_w$	217 ± 3	7×10^{-5}
After 50 cycles	$R_e(R_iQ_i)Q_w$	234 ± 3	5×10^{-5}
After 75 cycles	$R_e(R_iQ_i)Q_w$	247 ± 3	3×10^{-5}
After 100 cycles	$R_e(R_iQ_i)Q_w$	259 ± 4	4×10^{-5}
After 125 cycles	$R_e(R_iQ_i)Q_w$	271 ± 5	5×10^{-5}
After 150 cycles	$R_e(R_iQ_i)Q_w$	276 ± 5	4×10^{-5}
After 200 cycles	$R_e(R_iQ_i)Q_w$	300 ± 7	7×10^{-5}

Figure S10 shows the performance of a Li|B35|LFP cell cycled at 0.5C at 20 °C. The dis-/charge profiles are depicted in **Figure S10**a and the Nyquist plot recorded before cycling is shown in **Figure S10**b. The dis-/charge profiles reveal a discharge capacity of around 15 mAh g^{-1}, while the NLLS analysis of the Nyquist plot (inset in panel b) shows an associated interphase resistance as high as 1280 Ω, indicating an inferior interfacial contact and charge transfer at such lower temperatures, presumably owing to the more pronounced crystallinity of the PAN phase in the B35 membranes.

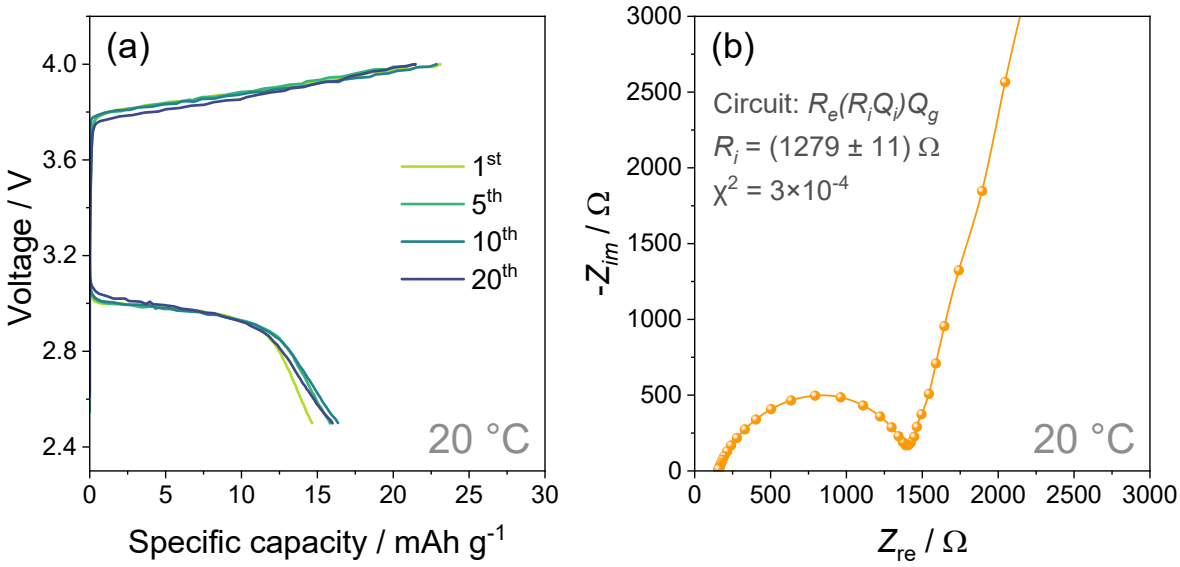

Figure S10. **(a)** Dis-/charge profiles of a Li|B35|LFP cell (LFP mass loading: 2.8 mg cm^{-2}) that was cycled at 0.5C between 2.5 and 4.0 V at 20 °C, and **(b)** the corresponding Nyquist plot recorded before cycling after a 12 h rest at the same temperature (the inset shows the NLLS analysis). EIS frequency range: 200 kHz – 50 mHz. Voltage amplitude: 10 mV.

Table S7 illustrates the comparison between the Li │SIPE │LFP cells investigated herein and other similar configurations reported previously. The table shows that the results achieved in this work are comparable with previous literature despite the relevantly higher LFP mass loading and the relatively lower cycling temperature, especially in comparison with other F-free formulations.

Table S7. Overview of previous Li │SIPE │LFP cells and comparison with the results presented in this work in terms of electrolyte composition, active material loading, cathode binder, cycling conditions, and performance.

Ionic function	Blending Polymer	LFP mass loading	Binder	Test conditions	Initial capacity	Capacity retention	Manuscript ref.
Sulfonyl-dicyanomethide	PAN (35 wt. %)	2.8 mg cm^{-2}	CMC	0.5C, 40 °C	114 mAh g^{-1}	76 % (500 cycles)	This work
Sulfonyl-dicyanomethide	PAN (35 wt. %)	9.2 mg cm^{-2}	CMC	0.2C, 40 °C	128 mAh g^{-1}	68 % (80 cycles)	This work
Borate	PEO (77 wt.%)	1.8 mg cm^{-2}	LA 133	1C, 55 °C	145 mAh g^{-1}	90 % (500 cycles)	48
Bis(benzene sulfonyl) imide	PVdF-HFP (50 wt.%)	0.9 mg cm^{-2}	PVdF	1C, 25 °C	110 mAh g^{-1}	96 % (200 cycles)	68
Bis(benzene sulfonyl) imide	PVdF-HFP (40 wt.%)	4-6 mg cm^{-2}	PVdF	1C, 25 °C	110 mAh g^{-1}	~100 % (800 cycles)	69
Bis(benzene sulfonyl) imide	PVdF-HFP (67 wt.%)	2.0 mg cm^{-2}	PVdF	1C, 25 °C	138 mAh g^{-1}	95 % (800 cycles)	70
Borate	-	1.7 mg cm^{-2}	PVdF	1C, 25 °C	136 mAh g^{-1}	91 % (500 cycles)	71
Bis(benzene sulfonyl) imide	PVdF-HFP (50 wt.%)	not provided	PVdF	1C, 25 °C	110 mAh g^{-1}	90 % (1000 cycles)	72
Perfluorosulfonimide	-	1.9 mg cm^{-2}	PVdF	0.1C, 40 °C	160 mAh g^{-1}	96 % (250 cycles)	25

References

1 M. Martinez-Ibañez, E. Sanchez-Diez, L. Qiao, L. Meabe, A. Santiago, H. Zhu, L. A. O'Dell, J. Carrasco, M. Forsyth, M. Armand and H. Zhang, *Batter. Supercaps*, 2020, **3**, 738–746.

2 H. Liang, M. Zarrabeitia, Z. Chen, S. Jovanovic, S. Merz, J. Granwehr, S. Passerini and D. Bresser, *Adv. Energy Mater.*, 2022, **12**, 2200013.

3 B. Boukamp, *Solid State Ion.*, 1986, **18–19**, 136–140.

4 B. Boukamp, *Solid State Ion.*, 1986, **20**, 31–44.

5 J. Evans, C. A. Vincent and P. G. Bruce, *Polymer*, 1987, **28**, 2324–2328.

6 M. Baumann, J. F. Peters, M. Häringer, M. Schmidt, L. Schneider, W. Bauer, J. R. Binder and M. Weil, *Green Chem.*, 2024, **26**, 6532–6552.

7 E. Abbate, A. M. J. Ragas, C. Caldeira, L. Posthuma, I. Garmendia Aguirre, A. C. Devic, L. G. Soeteman-Hernández, M. A. J. Huijbregts and S. Sala, *Integr. Environ. Assess. Manag.*, 2025, **21**, 245–262.

8 G. Rodriguez-Garcia, J. Braun, J. Peters and M. Weil, *Matér. Tech.*, 2017, **105**, 517.

9 L. G. Soeteman-Hernández, C. F. Blanco, M. Koese, A. J. A. M. Sips, C. W. Noorlander and W. J. G. M. Peijnenburg, *iScience*, 2023, **26**, 106060.

10 C. Caldeira, R. Farcal, I. Garmendia Aguirre, L. Mancini, D. Tosches, A. Amelio, K. Rasmussen, H. Rauscher, J. Riego Sintes and S. Sala, *Safe and sustainable by design chemicals and materials - Framework for the definition of criteria and evaluation procedure for chemicals and materials*, Publications Office of the European Union, Luxembourg, 2022.

11 Search for chemicals - ECHA, https://echa.europa.eu/information-on-chemicals.